ingegneria sismica
International Journal of Earthquake Engineering
Anno XLIII - Num. 2 - 2026

Design of data acquisition and optimal scheduling algorithm for air-conditioning equipment for grid supply-demand balance

Weishuai Wang[1], *Ze Zhang*[2,*], *Haichao Cui*[2], *Jinglan Cui*[2] *and Chao Gao*[2]

[1] State Grid Shandong Electric Power Company, Jinan, Shandong, 250001, China
[2] State Grid Dezhou Power Supply Company, Dezhou, Shandong, 253000, China

SUMMARY: *Load variations significantly influence the operational state of CCHP microgrids. To enhance the microgrids' capacity to handle power fluctuations, this paper presents a flexibility supply - demand balance indicator for the power system. Concurrently, it gathers energy consumption load data of air - conditioning systems.The flexibility supply/demand balance index serves to depict the degree of alignment between the supply of diverse flexibility resources and the system's flexibility requirements at different time intervals. A joint dispatch model of the power system, taking into account the flexibility supply - demand balance, is developed.The energy consumption variables of the air - conditioning system are managed. In the context of a regional multi - energy coupled system, the optimized scheduling performance of the joint scheduling model in terms of capacity allocation and annual comprehensive system revenue is examined. Different flexibility supply - demand matching coefficients are set to contrast the annual comprehensive income data across various cases. The trend of the annual comprehensive income is summarized, and the real - time dispatch outcomes of the joint dispatch model are analyzed from the viewpoints of electric energy storage and natural gas pipeline storage.When the flexibility supply - demand matching coefficients are set at 0.65, 0.85, 0.93, and 0.98, the comprehensive revenues of cases 1 - 4 are 4,207,646,200 yuan, 4,212,746,600 yuan, 4,221,311,100 yuan, and 4,161,127,400 yuan respectively. The comprehensive revenue in the system first rises and then falls as the flexibility supply - demand matching coefficients increase.The joint scheduling model can release electricity when the power system's energy supply is inadequate and store electricity when the energy supply is excessive. This enables the system to respond in real - time to the rapid fluctuations of wind power and ensure the balance of energy supply and demand within the system.*

KEYWORDS: *joint dispatch model; flexibility; supply-demand balance; annual integrated revenue; air-conditioning system energy consumption*

1 Introduction

As a large proportion of new - energy sources are integrated into the power grid, the issue of supply - demand balance in the power system has become more prominent. Moreover, the share of traditional power units is diminishing annually. This leads to a gradual decline in the regulatory capacity on the power - generation side of the power system. Meanwhile, the uncertainty on both the power - generation side and the user side has increased significantly.Consequently, the power balance of the power system will shift from the current

*zhangzedq0801@163.com
https://doi.org/10.65102/is2026596
Published: 30 April, 2026

deterministic balance to a probabilistic balance. This shift will bring about a series of challenges in the planning, scheduling, and operation of the power grid [1-5]. At the same time, with the progress of regulation technology, communication level and IoT technology, the controllability of the electricity load side is gradually improving [6]. In this regard, air conditioning loads have good dispatchable potential [7]. In the past few years, in some major urban regions, the proportion of air - conditioning loads during the summer peak electricity usage period can sometimes surpass 50%. This represents a significant portion of the energy consumption on the customer side [8]. Moreover, contemporary buildings typically possess superior thermal insulation capabilities. As a result, air - conditioning systems don't need to operate continuously for cooling. Air - conditioned rooms exhibit high thermal inertia. Under the condition of guaranteeing user comfort, power aggregation can be accomplished by slightly adjusting the set temperature of air - conditioning units [9 - 12].Consequently, air - conditioning loads, as active loads, engage in demand - side response to relieve the supply pressure on the power grid.

To guarantee the steady operation of air - conditioning systems and achieve a balance between the supply and demand of the power grid, it is necessary to conduct data collection and optimal scheduling of air - conditioning equipment. This helps to address the issue of the grid's stable operation under circumstances like the fluctuation and uncertainty of air - conditioning loads [13]. The approaches for collecting data on air - conditioning equipment can be classified into invasive and non - invasive load disaggregation methods. In reference [14], hourly data from smart meters were utilized to indirectly assess the energy consumption of air - conditioning in residential buildings. By applying the quartile theory and the change - point model to obtain the characteristics of base energy consumption and air - conditioning energy consumption from the smart meters, the air - conditioning energy consumption was dynamically estimated. Literature [15] designed a micro-vibration sensor with IoT functionality for air conditioning equipment, which is capable of capturing tiny vibration signals of air conditioning equipment, while ordinary sensors can capture parameters such as pressure, air flow and temperature. However, the installation cost and maintenance cost of the sensor and smart meter are high and the implementation is difficult. Reference [16] depicts the capability of non-invasive load decomposition technology in gathering and analyzing the electricity consumption data of residential customers. It addresses the issue of limited historical electricity consumption data accumulation by utilizing a non-invasive load decomposition approach founded on low-resource model migration.

In terms of air conditioning optimization and scheduling, it shifts from traditional optimization methods such as linear programming to artificial intelligence algorithms and hybrid optimization algorithms.Reference [17] devises a scheduling model for a solitary distributed inverter air - conditioning unit. It takes incentive compensation schemes into account, conducts clustering operations, and puts forward a load aggregation scheduling optimization strategy for inverter air conditioners that is oriented towards demand response. This strategy effectively cuts down the expenses associated with temperature compensation and load shedding for the loaders.In reference [18], a demand - response optimization scheduling model relying on direct load control is presented for air - conditioning systems in rural building complexes. This model makes use of genetic algorithms, long - and short - term memory neural networks. Its purpose is to regulate the peak air - conditioning load while ensuring a minimum level of thermal comfort. Literature [19] used machine learning to train the historical data of building air conditioning loads to achieve load prediction and proposed a cost optimal control strategy for air conditioning loads as a way to accomplish minimized air conditioning load scheduling. Literature [20] integrated frost and ice optimization algorithm, convolutional neural network, bi-directional gated recurrent unit algorithm, and attention

mechanism to develop a short-term air conditioning load forecasting and optimal scheduling algorithm, which reduces the cost of grid system operation. Reference [21] developed a multi - objective optimal scheduling model for air - conditioning loads using deep reinforcement learning. A proximal strategy optimization algorithm was incorporated to attain a dynamic equilibrium between economic effectiveness and thermal comfort, and to reduce the operating expenses of the distribution network to the lowest possible level.

This research paper conducts an in - depth examination of the supply - demand framework within the microgrid system. On the energy supply side, it constructs a model for photovoltaic batteries, a mechanism model for combined cooling, heating, and power (CCHP) systems, a model for ground - source heat pumps, and a model for energy storage devices. Meanwhile, on the demand side, it develops a model for translatable loads and a model for hot and cold loads.After analyzing the mechanism of flexible supply - demand equilibrium, separate modeling of flexible resources is carried out for the supply side, storage side, and demand side. Power system flexibility supply - demand balance indicators are introduced, and a source - load joint dispatch model is constructed and solved.Air conditioning equipment data is collected and pre - processed. In combination with regional grid system data, the optimization effect of the joint dispatch model that takes into account flexible supply - demand balance is analyzed. The intraday and real - time scheduling outcomes of energy storage and wind power consumption are compared to verify the real - time optimization scheduling effect of the joint scheduling model that considers flexible supply - demand balance.

2 Simulating the Supply - Demand Configuration and Adaptability of Microgrid Systems

The supply - demand configuration of the microgrid system developed in this research is depicted in Fig. 1. This system incorporates a Combined Cooling, Heating, and Power (CCHP) unit composed of a gas - driven turbine, a waste - heat steam generator, an absorption - type chiller, along with a heat pump and an energy storage apparatus. The system's input forms of energy encompass electricity, natural gas, and solar power sourced from the electrical grid. The outputs generated by this system are cooling, heating, and electrical energy. .

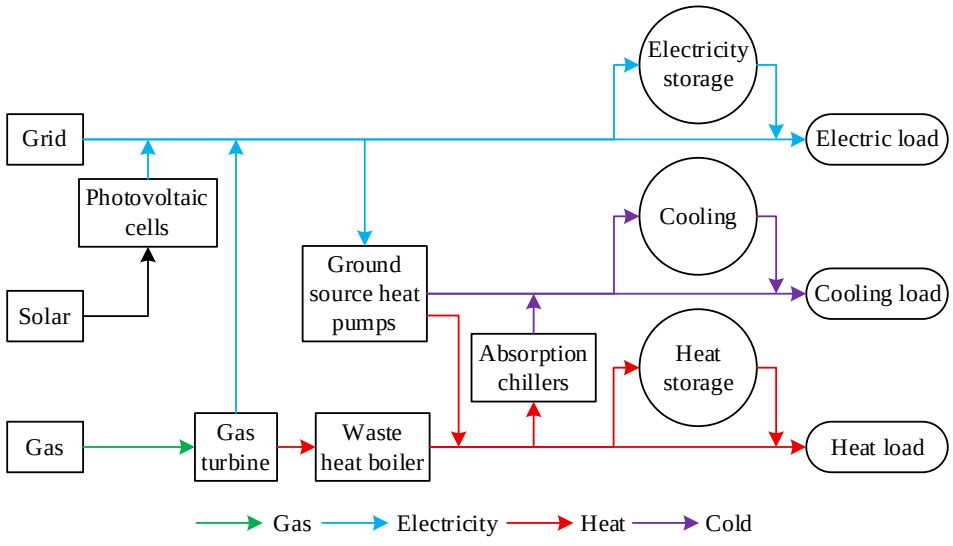

Figure 1: The supply and demand structure of micronetwork system

2.1 Supply-side modeling

2.1.1 Solar cell model

The output of the solar cell is primarily determined by the temperature of the cell's surface and the strength of solar radiation, as demonstrated in the subsequent equation:

$$P_t^{PV} = P_{Stc}^{PV} G_t \left[1+\gamma\left(T_t - T_{Stc}\right)\right]/1000 \tag{1}$$

where: P_t^{PV} is the power generated by the photovoltaic cell during the t hour. P_{Stc}^{PV} is the output power under standard test conditions ($1000\mathrm{W/m^2}, 25°\mathrm{C}$). G_t is the intensity of solar radiation at t time. γ is the power-temperature coefficient, T_t is the temperature of the surface of the PV cell at the t time period, and T_{Stc} is the reference temperature.

2.1.2 CCHP unit modeling

The Combined Cooling, Heating, and Power (CCHP) system incorporates a gas turbine, which burns natural gas to produce electricity. The waste heat produced during this process is captured by a waste - heat boiler. Subsequently, an absorption chiller makes use of this captured waste heat to cool the system, thereby achieving efficient energy utilization. The equations for the power output of electricity generation, the power associated with waste - heat recovery, and the power of the refrigeration process in the CCHP unit are presented in the following formula:

$$P_t^{GT} = \eta_{GT}^{e} \lambda_{gas} V_t^{GT} \tag{2}$$

$$H_t^{GT} = \eta_{WH}^{h} \left(1-\eta_{GT}^{e}\right) \lambda_{gas} V_t^{GT} \tag{3}$$

$$C_t^{Br} = I_c \lambda_t^{Br} H_t^{GT} \tag{4}$$

where: P_t^{GT}, H_t^{GT} are the power generated by the gas turbine and the heat power recovered by the waste heat boiler at t time respectively. $\eta_{GT}^{e}, \eta_{WH}^{h}$ are the gas turbine power production efficiency and the thermal power recovery efficiency of the waste heat boiler, respectively. V_t^{GT} is the amount of natural gas fed into the gas turbine during the t time period. λ_{gas} is the low calorific value of natural gas, and C_t^{Br} is the refrigeration power of the absorption chiller for the t time period. λ_t^{Br} is the proportion of thermal power input from the waste heat boiler to the absorption chiller in the t time period, and I_c is the refrigeration energy efficiency ratio.

2.1.3 Modeling of Ground - Source Heat Pumps

A ground - source heat pump can address the shortfall in flexibility associated with the thermoelectric coupling of a combined cooling, heating, and power (CCHP) unit. By consuming electrical energy to generate hot and cold energy, it can alter the thermoelectric ratio of the system. Here is the expression for its cooling and heating:

$$H_t^{HP} = COP_h P_t^{HP} \tag{5}$$

$$C_t^{HP} = COP_c P_t^{HP} \tag{6}$$

where: H_t^{HP}, C_t^{HP} are the heating and cooling power of the ground source heat pump in t time period respectively. P_t^{HP} is the electric power of the heat pump at time t. COP_h, COP_c are the energy efficiency coefficients of the heat pump for heating and cooling, respectively.

2.1.4 Modeling of energy storage equipment

Energy storage devices are added to microgrids to decouple thermoelectricity and realize energy leveling in time. General modeling of 3 types of energy storage devices for cold, heat and electricity, viz:

$$S_t^i = (1-\sigma_i) S_{t-1}^i (t-1) + \left[P_{ch,t}^i \eta_{ch,i} - \frac{P_{dis,t}^i}{\eta_{dis,i}} \right] \Delta t \tag{7}$$

where: S_t^i is the remaining capacity of the ith type of energy storage device in the tth hour. $P_{ch,t}^i, P_{dis,t}^i$ and $\eta_{ch,i}, \eta_{dis,i}$ are the charging and discharging powers and efficiencies of the energy storage device of the ith category in the tth time slot, respectively, and σ_i is the self-loss coefficient of the ith class of energy storage devices.

2.2 Demand-side modeling

2.2.1 Translatable Load Models

The levelable loads in the electrical loads have lower requirements for operation time, so the electricity consumption time of the levelable loads can be flexibly adjusted according to the system operation status. Electric load after calling the levelable load:

$$L_t^{new} = L_t^{ori} + u_t^{in} L_t^{in} - u_t^{out} L_t^{out} \tag{8}$$

where: L_t^{new} is the new load value after calling the levelizable load in t time period. L_t^{ori} is the original load forecast value for t time period. L_t^{in}, L_t^{out} are the values of transferring in and out of the level-shiftable load in the t time period, respectively, and u_t^{in}, u_t^{out} are 0-1 variables.

The shifted load operation should satisfy the power constraints as in Eq. (9), and the total load transfer in and load transfer out in each operation cycle should be equal. That is:

$$\begin{cases} \sum_{t=1}^{T} L_t^{in} = \sum_{t=1}^{T} L_t^{out} \\ 0 \leqslant L_t^{out} \leqslant \lambda_{out,\max} L_t^{ori} \\ 0 \leqslant L_t^{in} \leqslant \lambda_{in,\max} L_t^{ori} \\ u_t^{in} + u_t^{out} \leqslant 1 \end{cases} \tag{9}$$

where: $\lambda_{in,\max}, \lambda_{out,\max}$ are the maximum share of the transferred-in and transferred-out loads in the original load, respectively.

2.2.2 Hot and cold load modeling

Owing to thermal inertia, when the provision of heating and cooling energy is adjusted properly, the indoor temperature will not experience a sudden alteration. As a result, the heating and cooling loads are regarded as reducible loads, and the hot and cold loads are curtailed at peak loads, and at the same time, utilizing the complementary nature of the electric and thermal loads, the electric energy used for refrigeration and heating is reduced when there is insufficient supply of the electric loads, and the expression of loads after curtailment of the hot and cold loads:

$$Q_t^i = Q_t^{on,i} - Q_t^{cut,i} \tag{10}$$

where: Q_t^i is the new load value after the reduction of the cooling/heating load of the i category in the t time period. $Q_t^{ori,i}$ is the predicted value of the original cooling/heating load of the i class in the t time period, and $Q_t^{\mathrm{cut},i}$ is the value of the cooling/heating load curtailment with power constraints in the t time period:

$$0 \leqslant Q_t^{cut,i} \leqslant Q_{\max}^{cut,i} \tag{11}$$

where: $Q_{\max}^{cut}$ is the maximum amount of load that can be cut for the ith category of cooling/heating load.

2.3 Flexible resource modeling

In the power system, the flexible equilibrium of supply and demand is characterized as a mechanism capable of rapidly and effectively mobilizing diverse available resources within the power equilibrium over a specific time frame. This enables the system to achieve a flexible alignment between supply and demand. The concept of flexible supply-demand balance in power system can be extended to CCHP interconnected supply system.There are three forms of energy supply of cold, heat and electricity in the CCHP-type multi-microgrid system, and different energies are closely coupled with each other, so the construction of the flexibility balance for a certain kind of energy can be realized through the interaction of source-load-storage, and can also be realized by utilizing the energy complementarity between different loads. In addition, energy synergy between different microgrids can also enhance system flexibility.

2.3.1 Flexibility characterization

Because the grid structure of the distribution network is very complex, its nodes are also quite a lot, so the distribution of flexibility resources in the grid is also random and non-concentrated without regularity. Therefore, according to the mechanism that controls the balance between flexibility supply and demand, the distribution network has to ensure its network structure, that is the existing path, keeps unblocked as a basic requirement. Furthermore, through considering the structure characteristics of the distribution network, it can be confirmed that the distribution network's power load is affected by very many kinds of factors.

From the structure of the distribution system, it is evident that apart from the impact of the

distribution network itself, there are also the effects of renewable energy integration into the grid and the influence of diverse loads from the user end. As the degree of renewable energy penetration in the distribution network has been on the rise, the variability of the net load in the distribution network has been increasing. Moreover, with the advancement of new - energy technologies and the growing prevalence of numerous new - energy products, the loads at the customer level are becoming increasingly diverse. For instance, the rapid growth and utilization of various loads like household air - conditioners further exacerbate the volatility and uncertainty during the operation of the distribution network.Beyond these factors, during the actual operation of the distribution network, there will be a multitude of disruptions and malfunctions, which will exert a certain influence on the flexibility of the distribution network.

The distribution network's flexibility exhibits six primary traits: multi - temporal and multi - spatial features, directionality, state reliance, two - way conversion, probabilistic attributes, value, and physical properties.

Through an in - depth analysis of the traits of flexibility, the flexible resources within the distribution network are comprehensively investigated. When taking into account the network aspect, the power aspect, and the load aspect, the primary flexible resources include energy storage systems, adjustable loads, intelligent soft switches, and the superior main network.

2.3.2 Supply-side flexibility resources

(1) Gas boilers:

$$V_{GB} L_N \eta_{GB}^h = P_{GB.h} \cdot \Delta t \tag{12}$$

$$P_{GB}^{\min} \leqslant P_{GB.h} \leqslant P_{GB}^{\max} \tag{13}$$

where $P_{GB.h}$ is the heat production power of the gas boiler, L_{NG} is the calorific value of the gas, V_{GB} is the volume of gas consumed by the gas boiler, $P_{GB,g}$ is the power of the boiler's gas consumption, and η_{GB}^h is the heating efficiency of the gas boiler, and $P_{GB}^{\min}, P_{GB}^{\max}$ are the upper and lower limits of the power of the gas boiler, respectively.

(2) Gas turbine:

$$\begin{cases} V_{GT} \eta_{GT}^e L_{NG} = P_{GT \cdot e} \Delta t \\ P_{GT.e} = \eta_{GT}^e P_{GT.g} \\ P_{GT.h} = P_{GT.e} \cdot \gamma_{he} \\ P_{GT}^{\min} \leqslant P_{GT.g} \leqslant P_{GT}^{\max} \end{cases} \tag{14}$$

where V_{GT} is the volume of gas consumed by the gas turbine, $P_{GT.e}$ is the electrical output power of the gas turbine, $P_{GT.g}$ is the gas consumption power of the gas turbine, η_{GT}^e is the gas turbine power generation efficiency, $P_{GT.h}$ is the gas turbine heat production power, $\gamma_{h/c}$ is the gas turbine thermoelectric ratio, and $P_{GT}^{\min}, P_{GT}^{\max}$ are the upper and lower limits of gas turbine electric power, respectively.

2.3.3 Storage-side flexibility resources

The flexibility resources on the energy storage aspect of the microgrid possess significant scheduling capabilities. By making rational use of these flexibility resources on the energy storage side, the energy storage system can store or discharge electricity. This helps to balance the load of the microgrid and fulfill the power supply needs when the supply and demand sides of the microgrid cannot achieve equilibrium. In other words:

$$S_t^{ES} = \left(1-\mu_e\right) S_{t-1}^{ES} + \eta_{ch}^{e} P_t^{e,ch} - \frac{P_t^{e,dis}}{\eta_{dis}^{e}} \tag{15}$$

$$S_{ES}^{\min} \leqslant S_t^{ES} \leqslant S_{ES}^{\max} \tag{16}$$

where S_t^{ES} is the amount of power stored at time t, μ_c is the self-discharge rate, S_{t-1}^{ES} is the charging and discharging energy at $t-1$, $P_t^{e,ch}, P_t^{e,dis}$ is the charging and discharging power, $\eta_{ch}^{e}, \eta_{dis}^{e}$ is the charging and discharging efficiency, and $S_{ES}^{\min}, S_{ES}^{\max}$ is the upper and lower limits of power storage for the power storage device.

Energy storage devices need to meet the following constraints:

$$\begin{cases} S_{\min^i} \leqslant S_t^i \leqslant S_{\max^i} \\ 0 \leqslant P_t^{i,ch} \leqslant U_t^{ch} P_{ch}^{i-\max}; 0 \leqslant P_t^{i,dis} \leqslant U_t^{dis} P_{dis}^{i-\max} \\ 0 \leqslant U_t^{ch} \leqslant 1; 0 \leqslant U_t^{dis} \leqslant 1 \\ U_t^{ch} + U_t^{dis} \leqslant 1 \end{cases} \tag{17}$$

where $S_{\max^i}, S_{\min^i}$ are the maximum and minimum energy storage capacity of the microgrid i energy storage device, respectively, $P_{ch}^{i-\max}, P_{dis}^{i-\max}$ are the maximum charging and discharging power of the microgrid i energy storage device, respectively, U_t^{ch}, U_t^{dis} are the state quantities characterizing the charging and discharging of the microgrid i energy storage device, respectively.

2.3.4 Demand-side flexibility resources

(1) Electric load flexibility resources

Loads within the electrical load category that can be leveled have less stringent requirements for operating time. As a result, the period during which these levelizable loads consume electricity can be adjusted in a flexible manner based on the operational state of the system.The electric loads and constraints after the call of the levelable loads are as follows:

$$P_t^{eload} = P_t^{e0} + u_t^{ein} P_t^{ein} - u_t^{cout} P_t^{eout} \tag{18}$$

$$\begin{cases} \sum_{t=1}^{T} P_t^{ein} = \sum_{t=1}^{T} P_t^{eout}; u_t^{cin} + u_t^{cout} \leqslant 1 \\ 0 \leqslant P_t^{cout} \leqslant P_{\max}^{cout}; 0 \leqslant P_t^{cin} \leqslant P_{\max}^{cin} \end{cases} \tag{19}$$

where P_t^{eload} is the value of load after flexibility call at moment t, P_t^{c0} is the value of the original load prediction at moment t, P_t^{cin}, P_t^{cout} are the values of load transferring in and

out of the load at moment t respectively, u_t^{cin}, u_t^{cout} are 0-1 variables, and $P_{\max}^{cout}, P_{\max}^{cin}$ are the load transfer-in and transfer-out limits at time t, respectively.

(2) Heat load flexibility resources

In this paper, the thermal load stimulates the user to respond to the system scheduling through the incentive-based demand response, and the load expression after the thermal load response is as follows:

$$Q_t^{hload} = Q_t^{ho} - Q_t^{hcut} \tag{20}$$

$$0 \leqslant Q_t^{hcut} \leqslant Q_{\max}^{hcut} \tag{21}$$

where Q_t^{hload} is the heat load after flexibility call at moment t, Q_t^{ho} is the predicted value of the original cooling/heating load at moment t, Q_t^{hcut} is the heat load reduction value at moment t, and $Q_{\max}^{hcut}$ is the limit of the heat load that can be reduced.

3 Integrated dispatch framework that considers the equilibrium of flexibility supply and demand

3.1 Equilibrium of the supply and demand for flexibility within the power system

This research paper presents the power system flexibility supply - demand equilibrium index. This index is used to describe the level of compatibility between the provision of diverse flexibility resources and the system's flexibility requirements. These requirements are considered across different time scales and in multiple aspects related to the power source, power grid, load, and energy storage.

To measure the balance between the supply and demand of flexibility in the power system, the disparity between the upward and downward grid flexibility supply and demand at a specific moment is utilized. The calculation method is as follows:

$$\begin{cases} F_{n,S,t}^{U} = F_{n,f,t}^{U} - F_{n,N,t}^{U} \\ F_{n,f,t}^{U} = F_{n,G,t}^{U} + F_{n,ess,t}^{U} \end{cases} \tag{22}$$

$$\begin{cases} F_{n,S,t}^{D} = F_{n,f,t}^{D} - F_{n,N,t}^{D} \\ F_{n,f,t}^{D} = F_{n,G,t}^{D} + F_{n,ess,t}^{D} \end{cases} \tag{23}$$

where: n is the scene flag variable. $F_{n,S,t}^{U}$ and $F_{n,S,t}^{D}$ denote the upward and downward adjustments of the flexibility supply-demand balance indicator in the nth scenario at the tth moment, and $F_{n,f,t}^{U}$ and $F_{n,f,t}^{D}$ denote the upward and downward adjustments of the flexibility supply-demand balance indicator in the nth scenario at the tth moment, respectively. Flexibility supply. $F_{n,G,t}^{U}$ and $F_{n,G,t}^{D}$ denote the upward and downward flexibility that can be supplied by thermal power units, and $F_{n,ess,t}^{U}$ and $F_{n,ess,t}^{D}$ denote the upward and downward flexibility that can be supplied by energy storage devices, respectively.

$F_{n,N,t}^{U}$ and $F_{n,N,t}^{D}$ denote the up- and down-regulation flexibility demand of the power system at the t moment of the nth scenario, respectively.

Based on the definition of the flexibility supply - demand equilibrium index, for the system to stay in a state of flexibility supply - demand equilibrium, the flexibility supply ought to be marginally greater than the flexibility demand. This guarantees that the system can promptly make adjustments and uphold stable operation when confronted with fluctuations in power supply and demand.

3.2 Joint source-load scheduling model

3.2.1 Objective function

In this paper, an optimal dispatch model is established with the objectives of minimizing the cost $F_{n,1}$ of thermal power units, the cost of economic penalties and the cost of storage operation $F_{n,2}$, the cost of electricity-to-gas equipment operation $F_{n,3}$, as well as the integrated flexibility deficiency rate $F_{n,4}$. The multi-objective model is solved by normalizing it and assigning weighting coefficients, weighted summation is converted into a single objective function for solving, and the objective function F is as:

$$\min F = \sum_{n\in\Omega} \chi_n \left(\mu_1 \frac{F_{n,cco} - F_{n,\min}^{eco}}{F_{n,\max}^{eco} - F_{n,\min}^{eco}} + (1-\mu_1) \frac{F_{n,4} - F_{n,\min}^{flex}}{F_{n,\max}^{flex} - F_{n,\min}^{flex}} \right) \tag{24}$$

Among them:

$$F_{n,eco} = F_{n,1} + F_{n,2} - F_{n,3} \tag{25}$$

where: $F_{n,eco}$ is the integrated operating cost of the system. $F_{n,\max}^{eco}$, $F_{n,\min}^{eco}$ are the upper and lower bounds of the total operating cost, and $F_{n,\max}^{flex}$, $F_{n,\min}^{flex}$ are the upper and lower bounds of the inflexibility deficiency rate. μ_1 is the set of typical scenarios for wind and light loads. χ_n is the probability of occurrence of the corresponding scenario.

(1) Thermal power unit cost $F_{n,1}$

The power generation cost of thermal power units is much higher than the power generation cost of renewable energy mainly wind power and photovoltaic, so this paper ignores the power generation cost of renewable energy generation. The operating cost $F_{n,1}$ of thermal power units includes the heat standby cost and fuel generation cost, which is calculated as:

$$F_{n,1} = C_{n,g}\left(P_{n,g,t}\right) + C_{n,g}^{R} \tag{26}$$

where $C_{n,g}\left(P_{n,g,t}\right)$ is the unit's fuel generation cost and $C_{n,g}^{R}$ is the unit's hot standby cost.

(2) Economic penalty cost and storage operating cost $F_{n,2}$

The objective function $F_{n,2}$ is calculated as:

$$F_{n,2} = F_{n,RES} + F_{n,load} + F_{n,ess} \tag{27}$$

where: $F_{n,RES}$ is the system cost of wind and light abandonment, $F_{n,load}$ is the cost of lost load, and $F_{n,ess}$ is the operating cost of the energy storage device.

(3) Electricity-to-gas device operating cost $F_{n,3}$

Consider the operating cost $F_{n,3}$ of the P2G equipment which is mainly the revenue generated from the sale of natural gas $C_{n,P2G}$. It is calculated as follows:

$$F_{n,3} = C_{n,P2G} \tag{28}$$

3.2.2 Constraints

(1) Consumer Electricity Consumption Constraint

This limitation is intended to regulate the alterations in the overall quantity of electricity usage by consumers and uphold the secure and steady functioning of the power grid subsequent to the execution of price - based demand response. Namely:

$$\sum_{t=1}^{24} P_{n,Load,t}^{T} \sum_{k=1}^{10} \beta_{n,k} \eta_{n,kt} \geq \sum_{t=1}^{24} P_{n,Load,t}^{T} \tag{29}$$

(2) Operational limitations of energy storage devices

In the scheduling model presented in this paper, the operational limitations of the energy storage device are as follows. These constraints cover aspects such as the power limitations for charging and discharging the energy storage, the restrictions on the state of charge of the energy storage, the constraints on the initial and final states of charge of the energy storage, and the limitations on the charging and discharging states of the energy storage device at the same time instant:

$$0 \leq P_{n,r,t} \leq P_{\max}^{ess} \tag{30}$$

$$-PP_{\max}^{ess} \leq P_{n,d,t} \leq 0 \tag{31}$$

$$E_{n,t} = E_0 + \sum_{k=1}^{t} \left(P_{n,r,k} \delta_{n,k}^{r} \Delta t + P_{n,d,k} \delta_{n,k}^{d} \Delta t \right) \tag{32}$$

$$E_{\min} \leq E_{n,t} \leq E_{\max} \tag{33}$$

$$\sum_{t=1}^{24} \left(P_{n,r,t} \delta_{n,t}^{r} \Delta t + P_{n,d,t} \delta_{n,t}^{d} \Delta t \right) = 0 \tag{34}$$

$$\delta_{n,t}^{r} + \delta_{n,t}^{d} + \delta_{n,t}^{idle} = 1 \tag{35}$$

where: $P_{\max}^{ess}$ is the maximum power allowed for charging and discharging of the energy storage device. E_0 is the initial charging state of the energy storage device, $\delta_{n,t}^{r}, \delta_{n,t}^{d}$ and $\delta_{n,t}^{idle}$ denote the flag variables of the charging, discharging and idling state of the energy storage device, and the three of them are all integer variables from 0 to 1. When any of the state's flag variables is set to 1, the energy storage device is currently in the operational state.

Similarly, if a state flag variable has a value of 1, the energy storage device is in operation at this time.

(3) Power balance constraint

$$P_{n,w,t} + P_{n,pv,t} + P_{n,g,t} = P_{n,load,t} + P_{n,d,t} + P_{n,r,t} + P_{n,P2G,t} \tag{36}$$

where: $P_{n,w,t}$ and $P_{n,pv,t}$ denote the actual output power of wind power and photovoltaic power at the moment of t, respectively. $P_{n,load,t}$ is the actual active load at t moment.

(4) Thermal power output constraint

The limitations of thermal power units encompass the constraints on the available capacity of thermal power units.thermal power unit output power upper and lower limits constraints as well as unit upward and downward climbing rate constraints, the specific expressions are as follows:

$$P_{n,G\min} \le P_{n,g,t} \le P_{n,G\max} \tag{37}$$

$$0 \le P_{n,G\max} \le P_{\max}^{G} \tag{38}$$

$$\begin{cases} P_{n,g,t+1} - P_{n,g,t} \le P_{n,G,t}^{U} \Delta t \\ P_{n,g,t} - P_{n,g,t+1} \le P_{n,G,t}^{U} \Delta t \end{cases} \tag{39}$$

where: $P_{\max}^{G}$ is the sum of active power of thermal motor assembly machine.

(5) Constraints on the balance index of supply and demand for flexibility in the power system

Given that the supply and demand of power within the power system are in a dynamic state, the electrical grid must set aside a specific amount of upward and downward flexibility buffer. This buffer is essential for dealing with a wide range of unforeseeable occurrences in the system, including load variations, generator malfunctions, and weather alterations. Consequently, the balance index of power system flexibility supply and demand has to meet certain criteria, which is presented as follows:

$$F_{n,S,t}^{U} \ge N_{safe} \tag{40}$$

$$F_{n,S,t}^{D} \ge N_{safe} \tag{41}$$

where: N_{safe} is the margin of safety for the power system flexibility supply-demand balance metric.

3.2.3 Model solving

Within this research paper, the standardization approach is employed to convert the multi - objective optimization issue into a single - objective optimization problem. Subsequently, the GUROBI optimization solver is utilized to address the source - load integrated optimization scheduling model. Optimization of thermal power unit costs $F_{n,1}$, economic punishment cost and energy storage operation cost $F_{n,2}$, DianZhuan gas equipment running cost $F_{n,3}$ and integrated flexibility rate of less than $F_{n,4}$ four objective function, it is concluded that the

optimal scheduling plan a few days ago, The solution process of the model is shown in Figure 2.

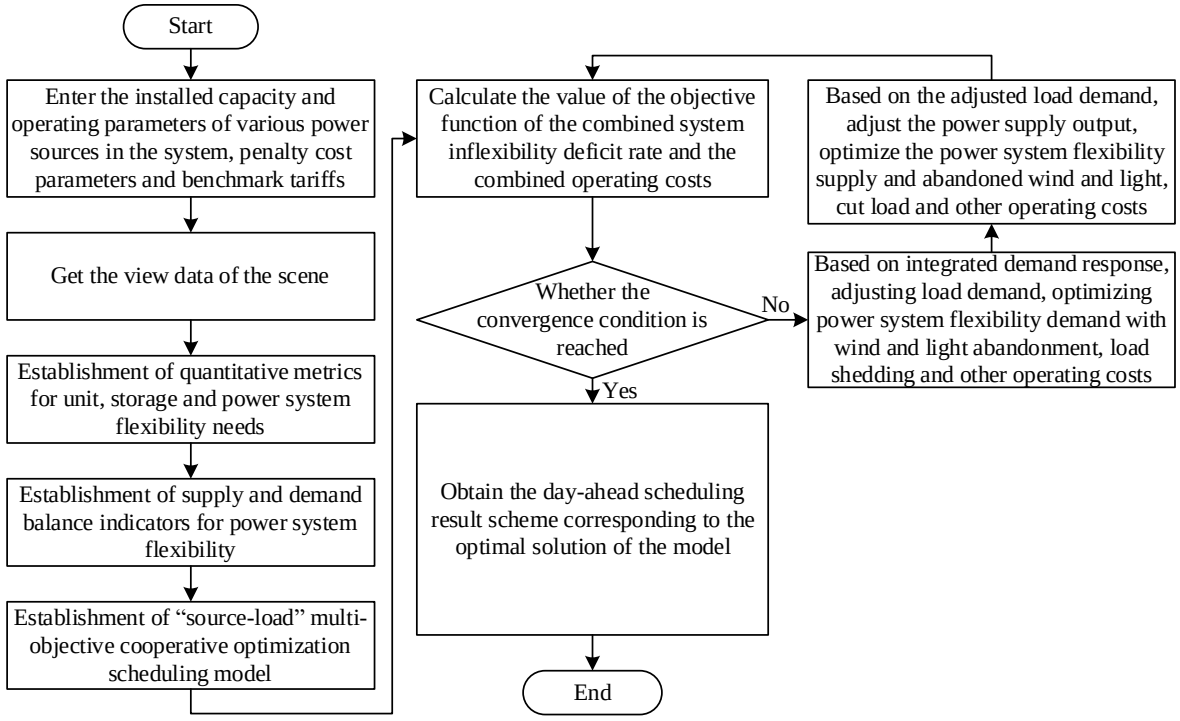

Figure 2: Model solving process

4 Simulation and analysis of results

4.1 Air Conditioning System Data Acquisition

The data comes from the measured data of an office building in the north, whose heating to the users is satisfied by the heat station. The thermal energy is conveyed to the heating station via the heat source. Subsequently, the heating station distributes this thermal energy to the end - users. The data collection period spans from November 10, 2024, to March 20, 2025, and the data collection interval is set at 10 minutes.

When the recorded instantaneous energy consumption in the original data is analyzed, it can be found that during the period of January 3, 2025-January 8, 2025, the value of instantaneous energy consumption remains constant. After analyzing the other variables, it can be found that variables such as flow rate in the high zone also remain constant. That is, it was not possible to construct the instantaneous heat for that day from the flow and temperature difference, and therefore, the data for those six days were given exclusion. After some preliminary processing, the data set has 14 variables with 4217 sets of samples, and the type of data, the range of data, and the unit of data are shown in Table 1.

Table 1: Data statistics

Variable class	Variable name	Variable range	Unit
Meteorological data	Outdoor temperature	[-15, 20]	℃
	Outdoor temperature	[-30, 5]	℃
	Relative humidity	[0.06, 1.00]	-
	Wind speed	[0.0, 66.3]	m/s
Running data	Secondary water supply temperature in high area	[28.3, 64.0]	℃
	Secondary water return temperature in high area	[29.5, 61.0]	℃
	Secondary water supply pressure in high area	[0.87, 1.01]	*kPa*
	High area secondary water return pressure	[0.73, 0.92]	*kPa*
	Low water return temperature	[38.5, 49.0]	℃
	Secondary water supply temperature in low area	[26.6, 47.2]	℃
	Secondary return water temperature in low area	[27.1, 48.7]	℃
	Secondary water return pressure	[0.36, 0.65]	*kPa*
	High zone instantaneous flow	[0.0, 26.2]	m^3 / h
	The current time is the instantaneous energy consumption interval	[-0.55, 254.8]	*kW*

4.2 System parameterization

In this special chapter, we will carry out simulation and analysis by taking a regional multi-energy coupling system as the example. This system, which is connected with a large-scale electric network, has heat power factories, photovoltaic power stations, wind fields and energy saving storage systems all joined at the same grid point B. To speak more specifically, the nominal working capacities of the photovoltaic power station and the wind power plant are 100 megawatts and 300 megawatts separately.

The parameters of each equipment device in the multi-energy coupling system are shown in Table 2.

Table 2: Equipment parameters

Equipment	Life/year	The cost of the loss/ (RMB / kW)	Flexibility call cost/ ($RMB / kW \cdot h$)
Fire electric unit	35	0.0495	0.0015
Photovoltaic equipment	25	0.0101	-
Wind power unit	15	0.0193	-
Energy storage equipment	10	0.0021	0.009

The pollutant emission factors and environmental penalty values in the system are shown in Table 3.

Table 3: Pollutant discharge coefficient and environmental punishment value

Contaminant	Pollutant discharge coefficient/ ($g / kW \cdot h$)	Environmental punishment value/ (RMB / kg)
CO	0.1120	1.021
CO_2	652	0.02943
Nitrogen oxide	2.93	8.80
SO_2	6.74	6.250

According to the operation rules of the Northern Electric Power Auxiliary Service Market, thermal power plants provide instant deep peak regulation services through the reduction of their output.That is, the feed-in tariffs for thermal power units when the average load factor is greater than or equal to 50%, between 40% and 50%, and less than or equal to 40% are 0.4 yuan $kW \cdot h$, 0.45 yuan $kW \cdot h$ and 1 yuan $kW \cdot h$, respectively.

The feed-in tariffs for thermal power, wind power and PV are shown in Table 4.

Table 4: Electricity, wind power and light volt

Average load rate	Fire power /($MRB / kW \cdot h$)	Wind power /($MRB / kW \cdot h$)	Photovoltaic /($MRB / kW \cdot h$)
≥50%	0.4	0.9	0.75
40%~50%	0.45	0.9	0.75
≤40%	1	0.9	0.75

4.3 Analysis of optimization results

4.3.1 Scene design

To validate the efficacy of the source - load joint scheduling model presented in this paper, which takes into account the flexibility supply - demand equilibrium, this section establishes three optimized allocation scenarios.

Scenario 1: For the power grid system, a conventional optimal allocation is carried out without taking into consideration the flexibility supply - demand matching within the system.

Scenario 2: The power grid system undergoes an optimized configuration while considering the flexibility supply - demand matching. In this scenario, thermal power units are regarded as flexibility supply equipment, and the flexibility supply - demand matching coefficient is greater than or equal to 0.9.

Scenario 3: An optimized configuration of the power grid system is implemented with the consideration of flexibility supply - demand matching. Here, both thermal power units and energy storage devices are treated as flexibility supply devices, and the flexibility supply - demand matching factor is greater than or equal to 0.9.

4.3.2 Capacity allocation in different scenarios

Figure 3 presents the outcomes of capacity allocation across three scenarios. When comparing these three configuration scenarios, it becomes evident that when the power grid system is optimally configured by taking into account the balance between the supply and demand of flexibility, there are significant changes in the configured capacities of thermal power units and energy storage equipment. Specifically, in comparison to Scenario 1, the configured capacity of thermal power units in Scenario 2 and Scenario 3 is reduced by 163.68 MW and 327.79 MW respectively, Conversely, the configured capacity of the energy storage

equipment experiences an increase of 27.65 *MW* and 101.33 *MW* respectively.

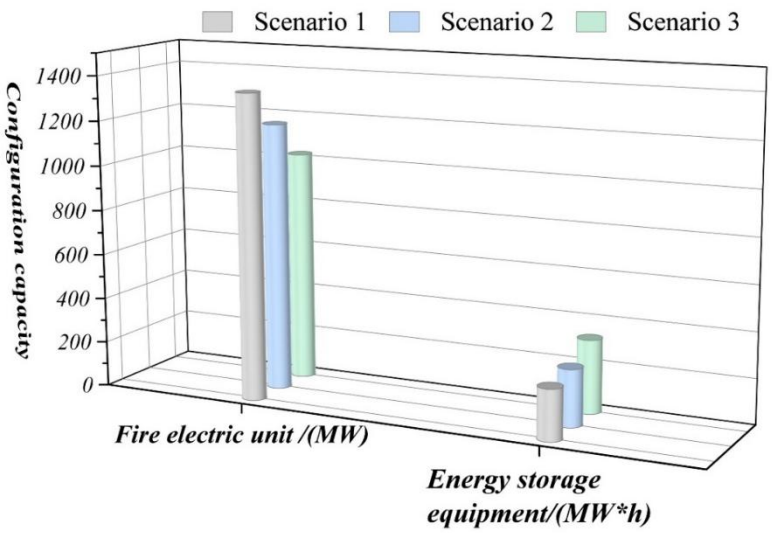

Figure 3: The capacity configuration results of the three scenarios

4.3.3 Annual consolidated system benefits under different scenarios

Figure 4 presents the outcomes of comparing the yearly comprehensive advantages of the system across three scenarios. Specifically, Figures (a) and (b) respectively illustrate the benefits and expenses under various scenarios. Among them, the flexibility supply-demand matching coefficient in Scenario 1, which considers traditional optimal allocation, is 0.6, and the flexibility invocation cost is 0.

The integrated benefits of the traditional optimal allocation scheme in Scenario 1 without considering flexibility supply-demand matching are optimal, while the integrated benefits of Scenario 2 and Scenario 3 are both lower than Scenario 1, and Scenario 3 has better benefits than Scenario 2. Among the revenues, thermal power units have the highest proportion of on-grid revenues, followed by wind power on-grid revenues, and PV on-grid revenues have a relatively low proportion of revenues.

Scenarios 2 and 3, which consider the flexibility of supply and demand matching, have the same PV on-grid revenue and wind power on-grid revenue, which are 155,236,800 yuan and 109,807,500 yuan, respectively, and both of them increase by 5.9% and 8.47% compared with Scenario 1, which does not consider the flexibility of supply and demand matching. As for thermal power units, Scenario 1, Scenario 2 and Scenario 3 are 2,748,565,600 yuan, 2,615,992,100 yuan and 2,705,360,700 yuan, respectively, while Scenario 2 and Scenario 3 have decreased by 1.57% and 0.05% respectively compared with Scenario 1 feed-in-targeting revenue.

Among the costs, the configuration investment cost accounts for the highest proportion, followed by O&M depreciation cost, penalty cost and flexibility call cost, and the environmental cost accounts for a relatively low proportion.

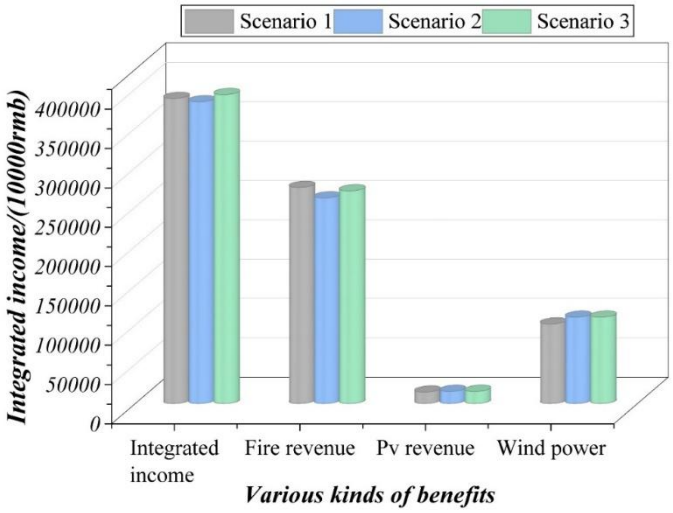

(a) Different benefits

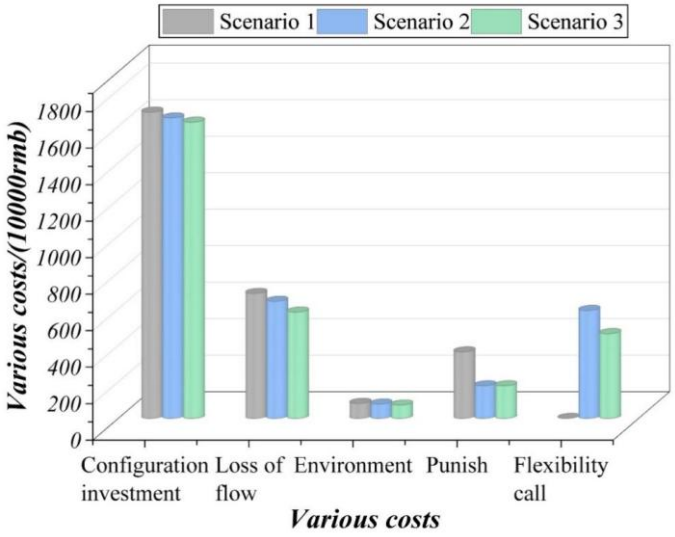

(b) Different cost

Figure 4: The comparison results of the system year in the three scenarios

4.3.4 Aggregate returns with different matching factors for supply and demand

To confirm the validity of the flexibility supply - demand matching coefficients put forward in this paper, an optimal configuration model of the grid system is utilized. By regarding thermal power units and energy storage devices jointly as flexibility supply devices, the annual comprehensive benefits corresponding to various flexibility supply - demand matching coefficients are calculated. Figure 5 presents the integrated returns associated with different flexibility supply - demand matching coefficients. It clearly shows that there are significant disparities in the system's annual integrated returns when meeting different flexibility supply - demand matching coefficients.

As the matching coefficient between flexible supply and demand rises, the overall profit within the system initially ascends and subsequently descends. Specifically, the overall profits of arithmetic cases 1 - 4 are 4,207,646,200 yuan, 4,212,746,600 yuan, 4,221,311,100 yuan,

and 4,161,172,400 yuan respectively. Among these profits, the on - grid profit of thermal power units, which has the largest proportion, first increases and then decreases as the flexible supply - demand matching coefficient goes up. Meanwhile, the on - grid profits of photovoltaic (PV) and wind power gradually increase with the rise of this coefficient.

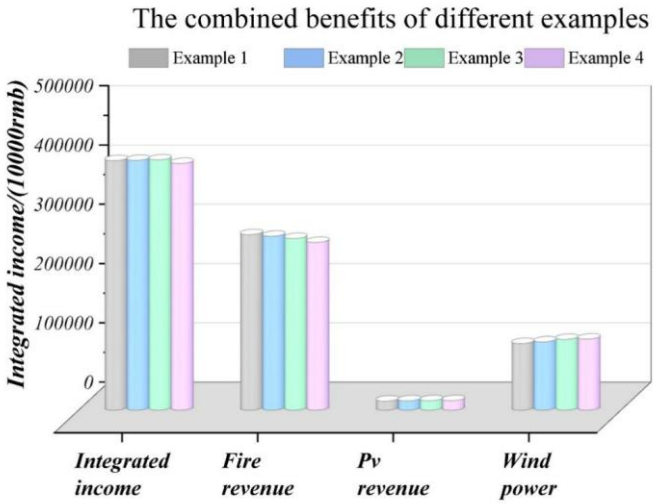

Figure 5: The comprehensive benefits of different flexibility of supply and demand

Table 5 presents the diverse kinds of costs corresponding to different coefficients of flexible supply - demand matching,and the total costs of configuration investment, O&M depreciation, environment, penalties, and flexibility invocation for the arithmetic examples 1-4 are 29.9413 million yuan, 29.4742 million yuan, 28.913 million yuan, 28.97150 million yuan, 28.9715 million yuan.

In the given examples, the expense of the flexibility call is on the rise. Meanwhile, the cost of configuration investment, which holds the largest proportion, experiences a slight decline as the flexibility supply - demand matching coefficient increases. This phenomenon can be attributed to the reduction in the capacity of the configured thermal power units.

Table 5: Various costs of different flexibility of supply and demand

	Example 1	Example 2	Example 3	Example 4
Flexibility supply and demand matching coefficient	0.65	0.85	0.93	0.98
Various costs/(10000rmb)				
Allocation of investment costs	1785.62	1725.18	1704.56	1684.26
The cost of the loss	583.95	557.36	523.21	514.37
Environmental cost	82.65	79.85	75.15	70.34
Cost of punishment	210.36	174.34	141.25	126.95
Flexibility call cost	331.55	410.69	445.96	501.23
Total cost	2994.13	2947.42	2890.13	2897.15
Benefits/(10000rmb)				
Overall income	423758.75	424222.08	425021.24	419014.39
Integrated income	420764.62	421274.66	422131.11	416117.24

4.4 Real-time phase scheduling

4.4.1 Algorithmic systems

In this research paper, a computational instance of an integrated energy system that combines electrical, gas, and thermal energy is developed. For the electrical system, the modified IEEE39 node model is employed, while the Belgian 20 - node model is utilized for the natural gas system. Considering the high transmission loss of heat network, which is not suitable for long-distance transmission, and the heat supply units usually only target a single area for heat supply, the regional heat network is equated to a nodal heat load.Moreover, the thermal energy is provided by the combined heat and power (CHP) units.

This calculation example system is followed and the number of units is modified by retaining one conventional thermal unit and adding four fast regulation units. On this basis the equivalent heat load is expanded into a 6-node thermal system. The thermal system contains three heat supply zones, which are supplied by two CHP units, with node 1 as the heat source node and nodes 4, 5, and 6 as the heat load nodes. The maximum and minimum temperatures of the supply pipe are 90°C and 60°C, respectively. For the return pipe, the maximum and minimum temperatures are 60°C and 30°C, respectively. Each heating zone's heating requirement is met at a temperature of 22°C with an allowable deviation of ± 5°C.

4.4.2 Movement control results

The real - time dispatching stage operates on a ten - minute time frame, which limits the regulation capacity of most conventional flexibility resources. Gas storage has a smaller response capacity and poorer dispatch timeliness at this time interval, so it is used as a backup regulation resource in the real-time dispatch phase. Considering the compressibility of natural gas gas, natural gas pipeline storage can provide some flexible regulation capability in the real-time phase of dispatch and work with electric system storage devices to cope with short-term fluctuations in power within the electric and gas energy systems. The example will analyze the real-time phase dispatch results from two perspectives: electric energy storage and natural gas pipeline storage.

Figure 6 presents a comparison of the operation of electric energy storage systems. The real-time dispatch phase curve increases again at 23h-24h electric storage capacity, and the 23h-24h electric storage capacity is in the range of 145.97MW~125.72MW. During the intraday scheduling phase, the peak of electric storage capacity occurs between 11h-12h, with a peak value of 276.86 MW. To address the minor power fluctuations resulting from prediction inaccuracies during the scheduling phase, the electrical energy storage device can promptly modify its charging and discharging status as well as the magnitude of the charging and discharging power. When the energy supply of the power system is inadequate, it releases power; conversely, when there is an energy surplus, it stores power. This allows the system to react to the rapid variations in wind power in real - time and safeguard the stability of wind power. As a result, the system can effectively handle the rapid wind - power fluctuations and maintain the equilibrium of energy supply and demand within the system.

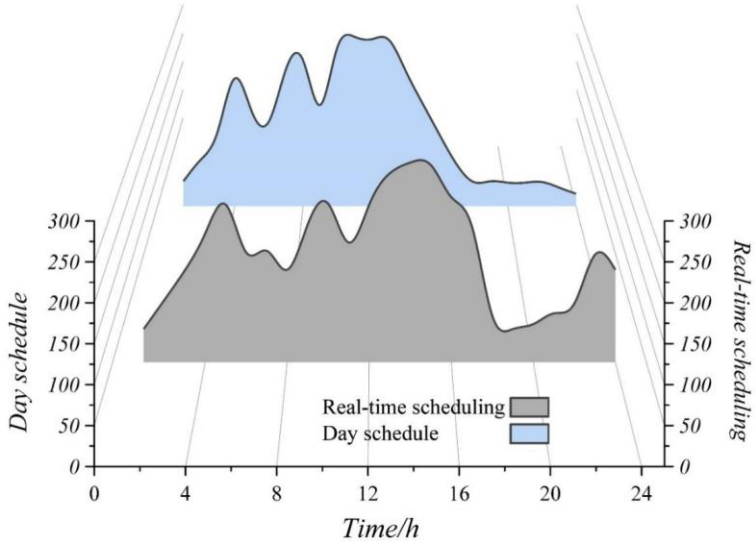

Figure 6: Comparison of electrical storage operation conditions

Figure 7 presents a comparison of wind power utilization. The wind power utilization curves during the intraday and real - time phases exhibit a largely similar trend. Between 0 - 4 hours and from 23 - 24 hours, there is a phenomenon of wind power curtailment. Nevertheless, the capacity of the energy storage devices is restricted,when it is full or storage capacity for the lower limit value, will no longer have the ability to cope with the regulation of power fluctuations in the system, at this time if you want to reduce the phenomenon of wind abandonment or cut load occurs, need to cooperate with the other energy system can be quickly responded to the flexibility of resources.

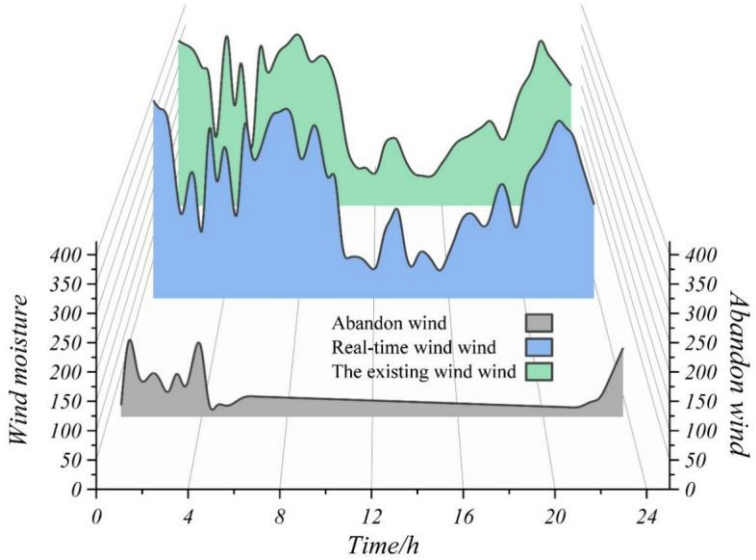

Figure 7: Comparison of wind power degradation

Figure 8 depicts the disparity between the net generation of the integrated equipment within the natural gas system and the alteration in the gas network pipeline inventory. The net gas consumption of the integrated equipment is computed by subtracting the gas output of the P2G unit from the combined gas consumption of the gas turbine and the CHP unit. Moreover, the term "difference" here denotes the gap between the real - time scheduling outcome and the intra - day scheduling outcome.

The peaks of the coupled unit net gas consumption difference curve and the gas network inventory change curve occur at 20h-24h.Between 22h-23h, , the peak value of the net gas consumption disparity for the coupled unit is -37.19 MW megawatts.and the maximum value of the gas network inventory change is 34.34 MW at 22h.The coupled unit net gas consumption difference and the gas network inventory change basically show an inverted characteristic, which is because in the real-time natural gas system phase of dispatch, without considering the role of gas source and gas storage regulation, the interaction between the natural gas system and other energy systems mainly relies on the energy coupling equipment, when the energy coupling equipment increases the natural gas consumption in response to power fluctuations in other energy systems, resulting in a shortage of natural gas supply, The natural gas pipeline infrastructure has the capacity to discharge a portion of the natural gas within the permitted pressure range. This can be achieved by reducing the volume of gas stored in the pipeline network, thereby easing the pressure on energy supply. Conversely, when the consumption of natural gas declines and there is an excess of gas, the excess can be temporarily stored through the compression of pipeline gas.The dynamic storage properties of the gas network offer dual benefits. Firstly, they enable the natural gas system to manage rapid power variations effectively. Secondly, they increase the regulatory scope of gas - electric coupling devices on short - term scales. As a result, the power system's ability to handle short - term power fluctuations is enhanced.

The outcomes of the simulation indicate that the joint dispatch model, which takes into account the equilibrium between flexibility supply and demand, can rapidly mitigate the short - term power fluctuations within the system. By leveraging the coordination and mutual assistance among the regulatory capacities of electrical storage, gas network pipeline storage, and other flexible resources, it can broaden the power regulation scope of the power system during the real - time dispatch phase. This is done to guarantee the precision of system scheduling.

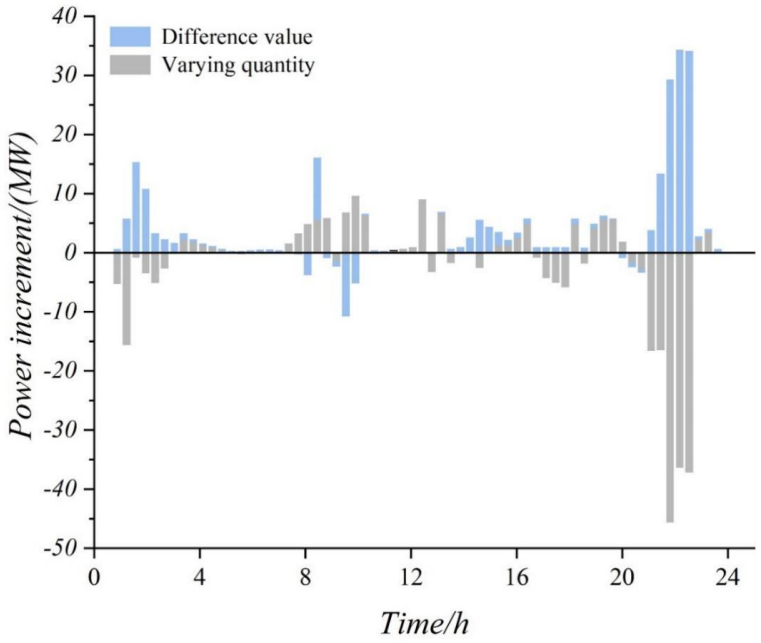

Figure 8: Gas system coupling equipment and air network

5 Conclusion

In this research paper, we construct models separately from the energy supply aspect, demand aspect, and flexible resources. We then establish the objective function and constraints, present the power system flexibility supply - demand balance indices, and develop a combined scheduling model that takes into account the balance between the flexibility supply and demand of the power system. Data from the air - conditioning system and the regional power grid system are gathered to conduct an analysis of the combined dispatch model.

(1)A variety of optimization scenarios are established. Regarding capacity allocation: when the grid system is optimized by taking into account the matching of flexible supply and demand, in contrast to Scenario 1, the allocated capacity of thermal power units in Scenario 2 and Scenario 3 is reduced, while the allocated capacity of energy storage equipment is increased.

When considering the annual overall revenue of the grid system, the photovoltaic (PV) on - grid revenue and wind power on - grid revenue in Scenario 2 and Scenario 3 are identical. The PV on - grid revenue amounts to 155,236,800 yuan, and the wind power on - grid revenue is 109,807,500 yuan. In comparison with Scenario 1, these revenues show an increase of 5.9% and 8.47% respectively. Conversely, the feed - in tariffs of the thermal power units in Scenario 2 and Scenario 3 experience a decline of 1.57% and 0.05% respectively when compared to those in Scenario 1.

The combined benefits vary under distinct flexibility supply - demand matching factors. As the flexibility supply - demand matching factor rises, the combined benefits within the system initially climb and subsequently decline.

(2) The integrated scheduling model that takes into account the balance between flexible supply and demand can instantaneously stabilize the power of the electrical system. It achieves this by making use of flexible resources like electrical energy storage and gas network pipeline storage. This ensures that the grid system, which includes air - conditioning, is scheduled precisely and promptly.

About the Author

Weishuai Wang born in 1988, from Fengxian County, Jiangsu Province, bachelor degree, currently working in State Grid Shandong Electric Power Company, research direction is electrical engineering and automation.

Ze Zhang born in 1990, from Dezhou, Shandong province, master's degree from North China Electric Power University. He is currently working in State Grid Dezhou Power Supply Company, specializing in electrical engineering and automation.

Haichao Cui born in 1987, from Wuqiao, Hebei province, bachelor degree from Three Gorges University. He is currently working at State Grid Dezhou Power Supply Company. His research direction is electrical engineering and automation.

Jinglan Cui born in 1994, from Haixing, Hebei province, bachelor degree from North China Electric Power University. She is currently working at State Grid Dezhou Power Supply Company. Her research direction is electrical engineering and automation.

Chao Gao born in 1995, from Dezhou, Shandong Province, master's degree from Northeastern University. He is currently working in State Grid Dezhou Power Supply Company, majoring in electrical engineering and automation.

References

[1] Yang, X., Zhang, Y., He, H., Ren, S., & Weng, G. (2018). Real-time demand side management for a microgrid considering uncertainties. IEEE Transactions on Smart Grid, 10(3), 3401-3414.

[2] Mayo-Maldonado, J. C., Valdez-Resendiz, J. E., & Rosas-Caro, J. C. (2018). Power balancing approach for modeling and stabilization of DC networks. IEEE Transactions on Smart Grid, 10(4), 4188-4200.

[3] Marneris, I. G., Roumkos, C. G., & Biskas, P. N. (2019). Towards balancing market integration: Conversion process for balancing energy offers of central-dispatch systems. IEEE Transactions on Power Systems, 35(1), 293-303.

[4] Gan, L., Jiang, P., Lev, B., & Zhou, X. (2020). Balancing of supply and demand of renewable energy power system: A review and bibliometric analysis. Sustainable Futures, 2, 100013.

[5] Rosales-Asensio, E., Diez, D. B., & Sarmento, P. (2024). Electricity balancing challenges for markets with high variable renewable generation. Renewable and Sustainable Energy Reviews, 189, 113918.

[6] Hong, J. H., Hong, D. Y., Yao, L. H., & Fu, L. C. (2020, November). A demand side management with appliance controllability analysis in smart home. In 2020 International Conference on Smart Grids and Energy Systems (SGES) (pp. 556-561). IEEE.

[7] Chen, X., Wang, J., Xie, J., Xu, S., Yu, K., & Gan, L. (2018). Demand response potential evaluation for residential air conditioning loads. IET Generation, Transmission & Distribution, 12(19), 4260-4268.

[8] Ran, B., Qiu, S., Zhang, Y., Zeng, L., Zhu, J., Xiang, Z., & Long, J. (2023). Air conditioning energy consumption measurement and saving strategy analysis for an office building in hot summer and cold winter area. Advances in Building Energy Research, 17(1), 73-97.

[9] Li, W., Yang, L., Ji, Y., & Xu, P. (2019). Estimating demand response potential under coupled thermal inertia of building and air-conditioning system. Energy and Buildings, 182, 19-29.

[10] Yang, Z., Dong, X., Xiao, H., Sun, H., Wang, B., Shi, W., & Li, X. (2022). Investigation of thermal comfort of room air conditioner during heating season. Building and Environment, 207, 108544.

[11] Zhang, L., Tang, Y., Zhou, T., Tang, C., Liang, H., & Zhang, J. (2022). Research on flexible smart home appliance load participating in demand side response based on power direct control technology. Energy Reports, 8, 424-434.

[12] Liu, J., He, C., Ding, Y., & Tan, J. (2025, March). Research on the Assessment of Potential and Scheduling Strategy for Air Conditioning Load Clusters Aggregation Response Considering Users' Comfort. In 2025 7th Asia Energy and Electrical

Engineering Symposium (AEEES) (pp. 900-906). IEEE.

[13] Zhu, Y., Tang, Z., Xu, Z., Zhao, J., Yu, M., Zheng, Q., & Wang, D. (2025). Optimising load control of multi-type air conditioning in demand-side management. Cyber-Physical Systems, 11(3), 347-369.

[14] Jin, X., Wang, S., Hu, Q., Zhang, Y., Qiu, P., Liu, Y., & Dou, X. (2024). Estimating air conditioning energy consumption of residential buildings using hourly smart meter data. Journal of Building Engineering, 97, 110729.

[15] Sung, M. F., Kuan, Y. D., & Chang, W. H. (2024). Design and Fabrication of IoT Sensor in Air-conditioning Equipment for Failure Mode and Effects Analysis. Sensors & Materials, 36.

[16] Lin, L., Shi, J., Ma, C., Zuo, S., Zhang, J., Chen, C., & Huang, N. (2023). Non-intrusive residential electricity load decomposition via low-resource model transferring. Journal of Building Engineering, 73, 106799.

[17] Li, Q., Zhao, Y., Yang, Y., Zhang, L., & Ju, C. (2022). Demand-response-oriented load aggregation scheduling optimization strategy for inverter air conditioner. Energies, 16(1), 337.

[18] Wei, Y. A., Meng, Q., Zhao, F., Yu, L., Zhang, L., & Jiang, L. (2024). Direct load control-based optimal scheduling strategy for demand response of air-conditioning systems in rural building complex. Building and Environment, 258, 111584.

[19] Guo, Z., Wang, X., Wang, Y., Zhu, F., Zhou, H., Zhang, M., & Wang, Y. (2024). The Cost-Optimal Control of Building Air Conditioner Loads Based on Machine Learning: A Case Study of an Office Building in Nanjing. Buildings, 14(10), 3040.

[20] Huang, Z., Peng, F., Li, D., Tao, J., Wang, W., & Zhang, L. (2025, August). Short-term Air Conditioning Load Forecasting and Optimal Scheduling Based on RIME Optimized CNN-BiGRU-Attention Model. In 2025 IEEE 20th Conference on Industrial Electronics and Applications (ICIEA) (pp. 1-6). IEEE.

[21] Zhao, Y., Ma, W., Liu, Z., Wang, X., Dou, J., & Li, T. (2025, July). Multi-Objective Optimization Scheduling of Air Conditioning Load Based on the PPO Algorithm. In 2025 7th International Conference on Power and Energy Technology (ICPET) (pp. 363-368). IEEE.